Solid Freeform Fabrication 2021: Proceedings of the 32nd Annual International Solid Freeform Fabrication Symposium – An Additive Manufacturing Conference
Reviewed Paper

Bayesian Process Optimization for Additively Manufactured Nitinol

Jiafeng Ye*, Mohammad Salman Yasin†, Muztahid Muhammad†, Jia Liu*, Aleksandr Vinel*, Daniel Silva*, Nima Shamsaei†, Shuai Shao†

*Department of Industrial and Systems Engineering, Auburn University, Auburn, AL 36849
†Department of Mechanical Engineering, Auburn University, Auburn, AL 36849

Abstract

Additively manufactured nitinol enables the design and rapid prototyping of the shape memory alloy with great flexibility and cost-effectiveness in various applications. To achieve high-density fabrication of nitinol, we utilize a Gaussian process-based Bayesian optimization method to efficiently optimize process parameters of the laser beam-powder bed fusion (LB-PBF) process in this work. Specifically, Gaussian process regression is applied to formulate a surrogate model between the critical process parameters (i.e., laser power, scanning speed) and the residual porosity of the nitinol samples. Then Bayesian optimization is integrated to successively explore the design space to search for the optimal process parameters. These two methods are integrated to find the global optimum iteratively. Compared with the traditional trial-and-error methods, the proposed method can quickly find the optimal process parameter for the high-quality nitinol samples, especially with many process parameters, and accelerate the innovations with nitinol in additive manufacturing.

Keywords: Nitinol, Laser beam-powder bed fusion, Process parameters, Bayesian optimization

1 Introduction

Nitinol (nickel-titanium alloy) typifies a generic class of shape memory alloys ranging in composition from 52 to 56 weight percent nickel and balance titanium [1]. They could undergo a large deformation (10-30 times as much as ordinary metal), remain in the deformed shapes when external forces being removed, and instantaneously restore to original shapes after being heated over transformation temperatures (known as “pseudoelasticity”) [1-5]. Moreover, nitinol has good biocompatibility to the human body [6-8] and has wide applications in medical devices, ranging from orthodontic, archwires, endoscopic instruments to endovascular stents [9]. Concurrently, the global nitinol medical devices market, evaluated at $14.52 billion in 2018, is projected to expand at a compound annual growth rate of 8.5% from 2019 to 2027 due to increasing demands for minimally invasive procedures [10].

The laser beam-powder bed fusion (LB-PBF) process is a promising additive manufacturing (AM) technology to provide customized nitinol medical products with reduced production ramp-up time and design customization [11]. This process has the following advantages: (1) No additional tool is needed when prototyping different products; (2) Unused

material could be recycled to reduce the overall material costs; (3) The product design is customizable through the computer-aided design.

However, researchers found that inappropriate fabrication conditions lowered the quality of nitinol products, which obstructed the applications of the LB-PBF process on nitinol [12-18]. More specifically, improper process parameters caused defects, cracks, and inferior surface quality of the LB-PBF fabricated nitinol products. An energy density E (J/mm^3) has been defined in Equation (1) with multiple process parameters in conjunction [19]:

$$E = \frac{P}{v \times h \times t} \tag{1}$$

where P is laser power (W), v is scanning speed (mm/s), h is hatch distancing (mm), and t is layer thickness (mm). Mahmoudi et al. [12] observed high porosity experimental samples with visible cracks when the energy density was lower than 30J/mm^3. Walker et al. [17] detected an increased number of defects on samples produced with constant laser power and rising scanning speed due to the low energy density. Contrarily, they observed that the high energy density, comprised of high laser power and low scanning speed, increased melt pool dynamics to negatively affect the powder deposition in successive layers, leading to low-density samples. Wang et al. [16] found large amounts of keyholes and gas pores in the sample fabricated with 120W laser power and 400mm/s scanning speed. The numbers of keyholes were reduced remarkably with a 900mm/s scanning speed in their follow-up experiments, indicating the high energy density was the primary reason. These defects, pores, and surface cracks due to unsuitable process parameters could be the main sites for crack initiation, which negatively affected the fatigue behavior of the nitinol products [20, 21].

Moreover, some inappropriate fabrication conditions could cause the chemical impurities of the nitinol products. Since nickel is more volatile than titanium at elevated temperatures, several works [16-18, 22] pointed out that nickel evaporated during the LB-PBF process when the energy density reached a higher value above 200J/mm^3. Biffi et al. [18] found that the nickel component decreased from 51% to 50.4% when the energy density increased from 63J/mm^3 to 300J/mm^3. Some research [22-24] indicated that a reduction of 0.85% of nickel content led to a 30ºC increase in the transformation temperature of nitinol. Therefore, the nickel evaporation during the LB-PBF process due to high energy density could handicap the pseudoelasticity property of the nitinol and their applications of thermal-activated products.

Since the relative density could reflect porosity levels and chemical impurities, many researchers searched for the process parameters of the LB-PBF process that produced high-density nitinol samples. In many works, experiments comprising different process parameters were conducted to find the optimal process parameters. Biffi et al. [18] ran 42 experiments involving seven unevenly distributed levels of laser power ranging from 30W to 175W and six levels of scanning speed from 500mm/s to 3000mm/s. The sample fabricated with 125W laser power and 1250mm/s scanning speed reached the highest relative density above 99%. Walker et al. [17] conducted 48 experiments to study the relationship between process parameters (i.e., laser power and scanning speed) and relative density of LB-PBF fabricated nitinol samples. Their experiments covered ranges of laser power (50W to 300W) and scanning speed (250mm/s to 2000mm/s). They used 250W laser power and 1250mm/s to fabricate the sample with the highest relative density (> 98%). Wang et al. [16] studied the effect of varying single process parameter on the relative density

of their nitinol samples. They set different levels for scanning speed, hatch distancing, and laser power and conducted 22 experiments in total to fabricate high-density samples (>99%) with an energy density of 41J/mm^3. Zhu et al. [15] fabricated nine nitinol samples under different conditions to build an analytical model based on the Eagle-Tsai simulation model. They used the analytical model to find an area of fabrication conditions free of defects such as keyholes, lack of fusion, and balling. They produced fully dense nitinol sample (>99%) with the process parameters in the defect-free area.

Besides experiments and simulations, several machine learning methods have been applied to improve the quality of LB-PBF fabricated nitinol products. Mehrpouya et al. [25, 26] used the artificial neural network (ANN) algorithm to predict functional properties of nitinol samples such as strain recovery ratio and transformation temperatures based on process parameters (i.e., laser power, scanning speed, and hatch distancing). Their ANN models achieved high accuracy (R^2 values above 0.97) on the test data. Mahmoudi et al. [12] utilized the linear discriminant analysis to predict the occurrences of surface cracks depending on the linear energy density (laser power/scanning speed) values. The accuracy of their model was above 90%. These models could accurately predict the functional properties of LB-PBF fabricated nitinol samples based on the process parameters, but they lack the capability to identify the optimal process parameters.

In summary, there are two primary limitations among the state-of-the-art fabrication of the nitinol products via the LB-PBF process: (1) Inappropriate process parameters result in the low relative density of the nitinol products, which cripples their functions and future applications; (2) The related studies conducted time-consuming and costly experiments to test the effects of different process parameters on the relative density. In this case, we propose a nonparametric Bayesian framework to address these limitations by systematically combining the fabrication of nitinol samples through the LB-PBF process with the machine learning and optimization procedure in a physical-based data-driven manner. The framework enables an efficient exploration within the design space of process parameters to find the optimal one that leads to the fabrication of high-density nitinol samples. Therefore, it could further unleash the potential of the LB-PBF process in nitinol applications.

2 Methodology

The objective of the Bayesian framework in the present work is to efficiently find the optimal process parameters (i.e., laser power and scanning speed) to fabricate high-density nitinol samples through the LB-PBF process. As shown in Figure 1, the proposed Bayesian framework encompasses developing the initial input-output dataset, applying the iterative process, and acquiring the optimal process parameters. The residual porosity (100% - relative density) values are used as the output in the initial dataset. These data enter the iterative process, which consists of the following steps: (1) A Gaussian process (GP)-based surrogate model builds a relationship between process parameters and relative residual porosity through prediction; (2) The Bayesian optimization explores the surrogate model to search for the optimal process parameters; (3) The Bayesian update adds data from new fabrications to the dataset and iterates from the first step. The iterative process ends when the Bayesian optimization results converge, which leads to the acquisition of the optimal process parameter.

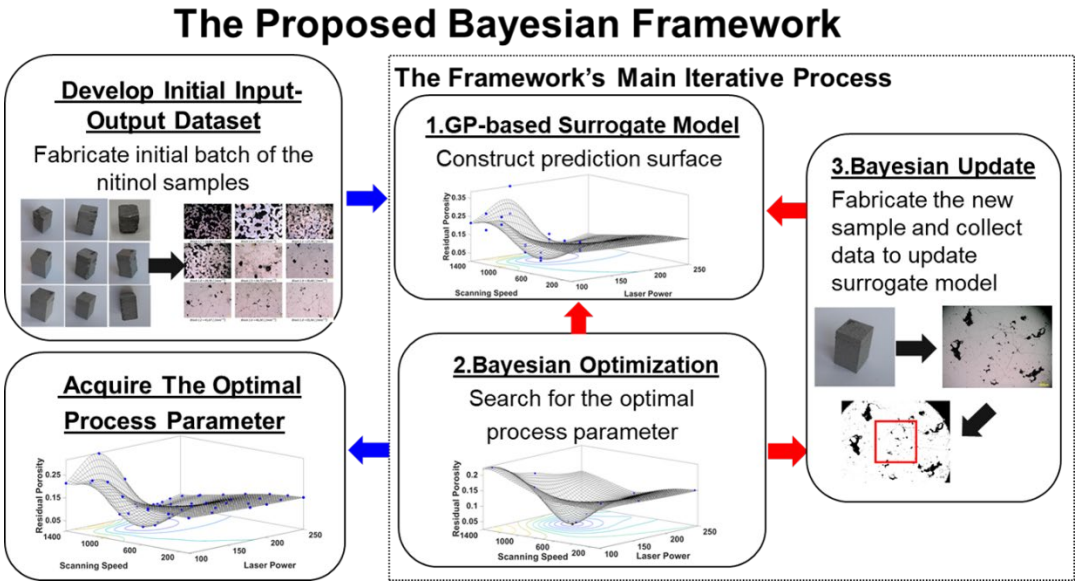

Figure 1. The steps of the proposed Bayesian framework to find the optimal process parameter for LB-PBF fabricated nitinol samples. The iterative process (red arrow) will be ceased when the Bayesian optimization results converge.

2.1 Gaussian process (GP)-based surrogate model

For the iterative process, we first utilize Gaussian process regression (GPR) to construct the surrogate model for mapping the nonlinear relationship between the process parameters and the residual porosity based on the initial input-output dataset. The GPR has been widely used to build computationally inexpensive (cost less than 1 minute) and high-accuracy (low mean absolute prediction error) surrogate models for process optimization in additive manufacturing [27-29]. Hence, we use the GPR to build the surrogate model for the Bayesian optimization to search for the optimal fabrication condition.

The GPR predefines a prior Gaussian distribution with mean μ and covariance C over the regression function f without a parametric form:

$$f \sim GP(\mu, C) \tag{1}$$

Our task is to utilize the function f to build the relationship between the process parameters $\boldsymbol{x}$ and residual porosity Y:

$$Y = f(\boldsymbol{x}) + \epsilon \tag{2}$$

In the present work, we assign the predictors $\boldsymbol{x}$ as the fabrication conditions of the nitinol samples, which consist of the laser power and scanning speed. ϵ is the random noise [27]. As a prior, GP furnishes a notion of similarity between the fabrication conditions using its covariance function $C(\cdot,\cdot)$ (e.g., exponential kernel function). Therefore, closer fabrication conditions lead to more similar residual porosity values, enhancing the predictive power of the GP-based surrogate model.

For modeling the fabrication conditions and residual porosity values, we establish training data comprising of various fabrication conditions $(\boldsymbol{x}_1, \boldsymbol{x}_2, \ldots, \boldsymbol{x}_n)$ and the random variables $\boldsymbol{f}_{training}$ of residual porosity values following a multivariate Gaussian distribution:

$$\boldsymbol{f}_{training} \sim \mathcal{N}\left(\boldsymbol{\mu}, \boldsymbol{\Sigma}_{training}\right) \tag{3}$$

where mean $\boldsymbol{\mu}$ is the expected porosity of the nitinol samples; the covariance function $\boldsymbol{\Sigma}_{training} = \boldsymbol{C}(\cdot,\cdot)$ encodes the correlations among the porosity variables $\boldsymbol{f}_{training}$ based on the similarity among their fabrication conditions $(\boldsymbol{x}_1, \boldsymbol{x}_2, \ldots, \boldsymbol{x}_n)$. For instance, one of the commonly used covariance functions is the exponential kernel function $C\left(\boldsymbol{x}_i, \boldsymbol{x}_j\right) = {\sigma_f}^2 exp\,(-\frac{r}{\sigma_l})$, where ${\sigma_f}^2$ is the signal standard deviation, and σ_l is characteristic length scale and $r = \sqrt{(\boldsymbol{x}_i - \boldsymbol{x}_j)^T(\boldsymbol{x}_i - \boldsymbol{x}_j)}$ as the Euclidean distance between conditions $\boldsymbol{x}_i$ and $\boldsymbol{x}_j$. It is usually assumed that more similar fabrication conditions result in a higher correlation among porosity via the kernel function.

The residual porosity as $\boldsymbol{f}'$ of test data at new fabrication conditions $(\boldsymbol{x}_1', \boldsymbol{x}_2', \ldots, \boldsymbol{x}_n')$ could be predicted by the GPR from the joint multivariate Gaussian distribution with the random variables $\boldsymbol{f}$ at fabrication conditions in training data [30].

$$\begin{bmatrix} f \\ f' \end{bmatrix} \sim \mathcal{N}\left[\begin{pmatrix} \mu \\ \mu' \end{pmatrix}, \begin{pmatrix} \boldsymbol{\Sigma} & \boldsymbol{\Sigma}_* \\ \boldsymbol{\Sigma}_*^{\mathrm{T}} & \boldsymbol{\Sigma}_{**} \end{pmatrix}\right] \tag{4}$$

where the $\boldsymbol{\Sigma}_*$ is the training-test covariance; $\boldsymbol{\Sigma}_{**}$ is the test data covariance. The conditional distribution of $\boldsymbol{f}'$ at new fabrication conditions can be written in terms of $\boldsymbol{f}$ as:

$$\boldsymbol{f}' | \boldsymbol{f} \sim \mathcal{N}(\overline{\boldsymbol{\mu}}, \overline{\boldsymbol{\Sigma}}) \tag{5}$$

where the mean function $\overline{\boldsymbol{\mu}} = \boldsymbol{\mu} + \boldsymbol{\Sigma}_* \boldsymbol{\Sigma}_{**}^{-1}(\boldsymbol{f}' - \boldsymbol{\mu}')$ and the covariance matrix $\overline{\boldsymbol{\Sigma}} = \boldsymbol{\Sigma} - \boldsymbol{\Sigma}_* \boldsymbol{\Sigma}_{**}^{-1} \boldsymbol{\Sigma}_*^{\mathrm{T}}$.

2.2 Bayesian optimization

We conduct the Bayesian optimization in a sequential design strategy to find the lowest predicted residual porosity value and its corresponding fabrication condition. This optimization algorithm attempts to find the global optimum in bounded design space with a minimum number of iterations and reduces the costly LB-PBF fabrications.

The objective function of the Bayesian optimization is to minimize the regression function $\boldsymbol{f}$ in Eq. (2) of the GPR. Bayesian optimization incorporates prior belief about $\boldsymbol{f}$ in a Gaussian process $GP(\mu, C)$ and updates the prior with observations to get a posterior that better approximates $\boldsymbol{f}$. An acquisition function is used to direct sampling to areas where an improvement over the current best observation is likely to occur.

Bayesian optimization maximizes acquisition function values based on the surrogate model to find the next sampling point $\boldsymbol{x}'$. The expected improvement (EI) is adopted as the acquisition function in this work, which is defined as the following equations:

$$\boldsymbol{x}' = \underset{\boldsymbol{x}}{\operatorname{argmax}}\ EI(\boldsymbol{x}) \tag{6}$$

$$\mathrm{EI}(\boldsymbol{x}) = \mathbb{E}\max(f(\boldsymbol{x}^+) - f(\boldsymbol{x}), 0)$$

where $f(\boldsymbol{x}^+)$ is the lowest residual porosity values of the nitinol samples so far under the fabrication condition $\boldsymbol{x}^+$. According to its definition, the EI acquisition function evaluates the expected amount of improvement in the objective function. It is often maximized with the implementation of Newton's Method.

A high exploration ratio t_σ has been incorporated into Bayesian optimization to prevent premature convergence by overexploiting an area. To illustrate the overexploiting, we assume $\sigma_F(\boldsymbol{x})$ is the standard deviation of the posterior objective function at condition $\boldsymbol{x}$. Let σ be the posterior standard deviation of the additive noise. The Bayesian optimization, after each iteration of the acquisition function, evaluates whether the next condition $\boldsymbol{x}'$ satisfies the following equation:

$$\sigma_F(\boldsymbol{x}') < t_\sigma \sigma \tag{7}$$

In consequence, the algorithm declares that area near condition $\boldsymbol{x}'$ is overexploiting. Correspondingly, the acquisition function modifies the kernel function by multiplying kernel parameters (σ_f and σ_l) with iteration numbers [31]. This adjustment enhances the correlation and similarity of nearby conditions, enabling the algorithm to exploit farther areas. In this work, we set a high t_σ value to encourage the algorithm to search for the potential optimal condition in the unexplored areas.

2.3 Bayesian update procedure

The Bayesian update procedure is iteratively integrated into the proposed framework to search for the global optimal fabrication condition. This procedure includes fabricating new samples based on predicted optimal conditions from the Bayesian optimization and collecting new data to update the surrogate model. The predicted optimal from an unexplored area tends to have a high variance, indicating high uncertainties. Hence, we fabricate new samples using the predicted optimal fabrication condition and collect new data to reduce the uncertainties of these unexplored areas in the surrogate model. The Bayesian optimization algorithm will explore the updated surrogate model to search for the optimal conditions for further new fabrications. This process is iterated until the optimization results converge, which indicates that the global optimum has been found.

There are several benefits for applying the developed Bayesian framework to the process optimization of LB-PBF fabricated nitinol samples. First, it reduces the number of experiments in finding optimal fabrication conditions. Compared to the full factorial design, which runs all combinations of process parameters, this Bayesian framework could work with fewer fabrications. For instance, a full factorial design with five levels of laser power and scanning speed requires twenty-five experiments in total. The full factorial design could result in exponentially increased experiments if new factors are added. In contrast, in the case study, the Bayesian framework starts with nine fabrications and needs approximately five iterations to find the optimal fabrication conditions, significantly improving the efficiency and reducing the experimental cost. As the framework concentrates on the areas which possibly include the optimal condition based on the

Bayesian optimization algorithm, there is no need to cover all combinations of process parameters through costly experiments. More importantly, the global optimal fabrication condition could be found through this framework. In contrast to finding the lowest residual porosity values from the surrogate model through interpolation, the EI acquisition function with a high exploration ratio t_σ could systematically explore the design space and prevent premature convergence of the optimization results.

In summary, the proposed Bayesian framework could find the optimal fabrication conditions for the LB-PBF process to produce high-density nitinol samples with a reduced number of fabrications. It could be easily extended to process parameter optimization in the LB-PBF process based on other required properties (i.e., transformation temperatures, elongation, tensile strength) for various applications, which entitles the proposed Bayesian framework great potential to improve the functional properties of the LB-PBF fabricated nitinol.

3 Case study

The proposed Bayesian framework is applied to a real-world case study to find the optimal process parameter of the LB-PBF process that fabricates high-density nitinol samples. In the case study, the nitinol samples are fabricated as cubic blocks. We fabricate these blocks through the LB-PBF process with different process parameters and correspondingly extract the residual porosity values to build the initial input-output dataset. Afterward, we conduct the iterative process of the proposed Bayesian framework with two more fabrications based on the Bayesian optimization result at each iteration. The case study result demonstrates the feasibility and effectiveness of the proposed Bayesian framework.

3.1 Data collection

An initial batch of 9 nitinol blocks (12.7mm×12.7mm×20mm) has been fabricated through the LB-PBF process with different fabrication conditions. These conditions cover a range of 100W to 200W of laser power and 1000mm/s to 1400mm/s of scanning speed. Since this work focus on the effects of the laser power and scanning speed on the residual porosity, the hatch distancing, and layer thickness are kept as 120 μm and 30 μm, respectively, throughout the whole process.

Figure 2 and Figure 3 display the finished nitinol blocks and their corresponding microstructure images. The microstructure images in Figure 3 demonstrate the effects of process parameters on the microstructure of the nitinol blocks. The blocks fabricated with an energy density lower than 30J/mm^3 (e.g., blocks 1.1, 1.4, 1.7, and 1.8) have inferior qualities with a large number of defects shown as the dark regions.

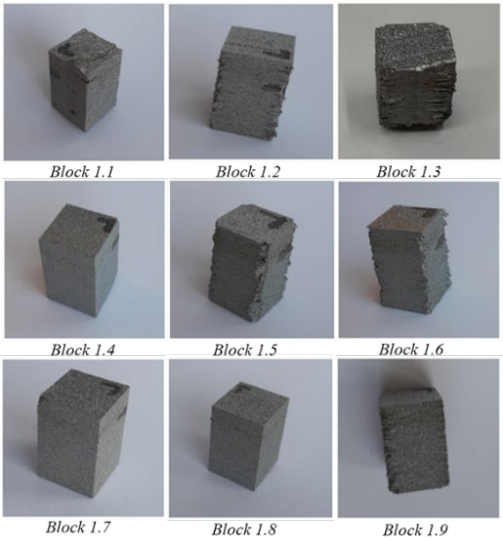

Figure 2. Images showing the finished nitinol blocks through LB-PBF under different fabrication conditions.

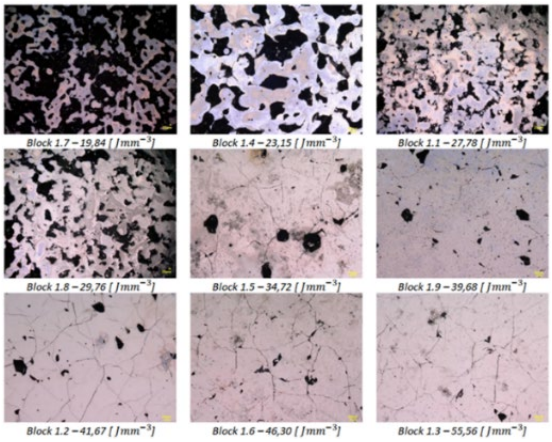

Figure 3. Microstructures as sectional views at X-Y direction of the nitinol blocks in the ascending order of energy density. The images show that blocks 1.7, 1.4, 1.1, and 1.8, fabricated with lower energy density values, have large amounts of defects shown as black regions.

The proportions of the defect region are quantified as the residual porosity values. These values are extracted from the microstructure images, binarized to separate the defects from normal printings. The observed residual porosity values of the nitinol samples and their fabrication conditions are summarized in Table 1. Several blocks (e.g., blocks 1.3, 1.5, and 1.6) have more values since they obtain more microstructure images.

Table 1. The fabrication conditions and corresponding residual porosity of the nitinol blocks. The bold number is the lowest residual porosity value detected from this batch of nitinol blocks.

Condition numbers	**Process parameters**			**Response**
	Laser power (W)	Scan speed (mm/s)	Energy density (J/mm^3)	Observed residual porosity (%)

1.1	100	1000	27.78	28.12	24.02	-	-	-
1.2	150	1000	41.67	**2.88**	5.60	-	-	-
1.3	200	1000	55.56	3.81	6.80	4.11	8.14	3.42
1.4	100	1200	23.15	28.29	19.33	-	-	-
1.5	150	1200	34.72	4.37	7.99	7.55	8.18	-
1.6	200	1200	46.30	4.12	5.04	3.27	7.26	-
1.7	100	1400	19.84	21.52	-	-	-	-
1.8	150	1400	29.76	38.48	23.52	-	-	-
1.9	200	1400	39.68	4.39	9.29	6.25	-	-

3.2 GP-surrogate model and Bayesian optimization

Figure 4 and Figure 5 illustrate the surrogate model and Bayesian optimization result at the first iteration of the framework. According to the prediction surface shown in Figure 4(a), the area where the laser power is from 140~200W and scanning speed from 1000~1200mm/s has the lowest predicted mean residual porosity values (<5%). However, it is noticeable that the predicted mean residual porosity values within this area have a standard deviation from 4~10% based on the estimated standard deviation shown in Figure 4(b). The lowest predicted mean residual porosity value of 0.78% is detected with a 4.3% standard deviation at the first iteration of the Bayesian optimization. The corresponding laser power is 150W, and the scanning speed is 1070mm/s.

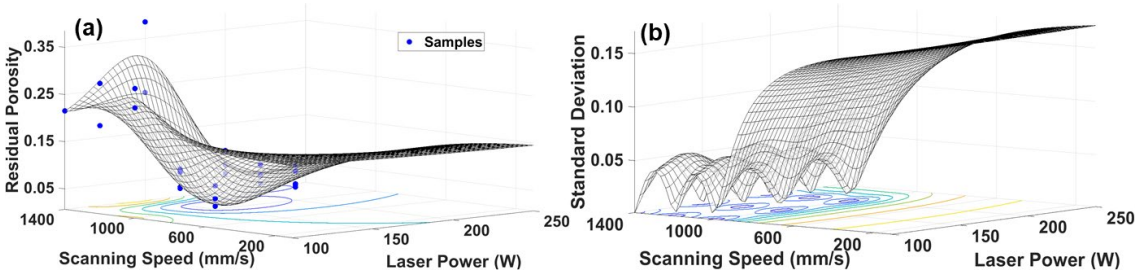

Figure 4. (a) The prediction surface of mean residual porosity from the surrogate model at different fabrication conditions. (b) The estimated standard deviation at different fabrication conditions from the surrogate model.

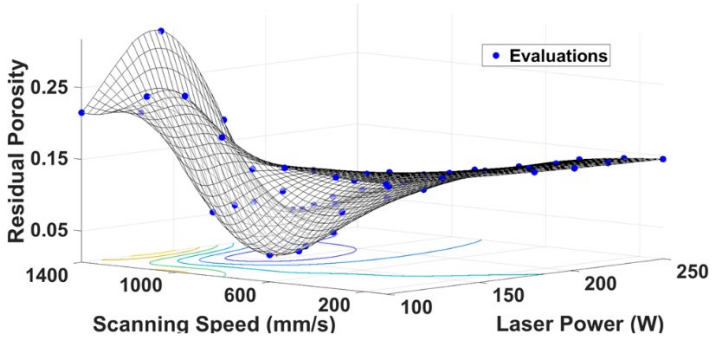

Figure 5. The first iteration of the Bayesian optimization with 50 evaluations to find the optimal fabrication condition. The lowest predicted mean residual porosity is 0.78% with 150W laser power and 1070mm/s scanning speed.

The results of the Bayesian optimization in terms of predicted optimal residual porosity values and their corresponding process parameters at each iteration are summarized in Table 2, comparing to the observed residual porosity values extracted from new fabrications. It can be seen that after the third iteration, the optimal mean residual porosity is 1.93%, with a corresponding fabrication condition of 163W laser power and 985mm/s scanning speed. The standard deviation showing the uncertainty of the prediction has been reduced to 1.21%, which indicates a higher prediction accuracy.

Table 2. The results for Bayesian optimization at each iteration. For each iteration, a predicted optimal mean residual porosity value and its standard deviation are given. New fabrications are conducted with these predicted optimal process parameters. The porosity values are observed from these newly fabricated parts and used to update the surrogate model in Bayesian optimization for the next iteration.

Bayesian optimization iteration	**Predicted optimal process parameters**			**Residual porosity**	
	Laser power (W)	Scan speed (mm/s)	Energy density (J/mm^3)	Predicted (Std.) (%)	Observed (%)
1	150	1070	38.94	0.78 (4.39)	2.43~7.63
2	160	970	45.81	1.55 (3.21)	2.36~6.18
3	163	985	45.96	1.93 (1.21)	-

Meanwhile, the observed residual porosity values have been reduced after the second iteration compared to the initial dataset, indicating that the quality of the nitinol block has been improved due to better fabrication conditions. Moreover, the optimal process parameters appear to converge after the second iteration with fewer changes than after the previous iteration. More iterations will be helpful to verify the convergence of process parameters.

4 Conclusion and future work

In this work, a nonparametric Bayesian framework incorporating prediction and optimization based on the GP and Bayesian optimization is proposed to discover the optimal laser power and scanning speed of the LB-PBF process for high-density nitinol manufacturing. The GP-surrogate model establishes the initial fabrication, and the Bayesian optimization leads to an efficient acquisition of optimal process parameters to fabricate high-density nitinol samples. The optimal process parameter trends to the convergence after a few iterations of the Bayesian framework. The framework can reduce the number of experiments in a data-driven manner and advance the innovations with nitinol in additive manufacturing.

The authors' future research will focus on the three aspects of this work:

(1) Additional iterations will be conducted to substantiate the convergence of optimization results and obtain the global optimal parameters (i.e., laser power and scanning speed) for LB-PBF fabricated nitinol samples.

(2) More process parameters will be involved in the proposed Bayesian framework, such as hatch distancing and layer thickness, which also affect the relative density of the LB-PBF fabricated nitinol samples. The proposed Bayesian framework could be expanded to more process parameters with a similar process. More importantly, including these process parameters could provide a more comprehensive understanding of the LB-PBF process to improve the reliability of the proposed Bayesian framework.

(3) The Batch Bayesian optimization method will be incorporated in the iterative process of the framework. The batch Bayesian optimization could provide a batch of different fabrication conditions within an area that may contain the optimal one. Since the batch production at different fabrication conditions is feasible for the LB-PBF process and more cost-effective than fabricating a single block. Thus, the application of batch Bayesian optimization will greatly enhance process parameter optimization for the additively manufactured nitinol.

References

[1] W. B. Cross, A. H. Kariotis, and F. J. Stimler, *Nitinol characterization study*. NASA, Langley Research Center, 1969.

[2] D. Stöckel, "Nitinol-A material with unusual properties," *Endovascular Update,* vol. 1, no. 1, pp. 1-8, 1998.

[3] N. B. Morgan, "Medical shape memory alloy applications—the market and its products," *Materials Science and Engineering: A,* vol. 378, no. 1, pp. 16-23, 2004/07/25/ 2004, doi: https://doi.org/10.1016/j.msea.2003.10.326.

[4] G. B. Kauffman and I. Mayo, "The Story of Nitinol: The Serendipitous Discovery of the Memory Metal and Its Applications," *The Chemical Educator,* vol. 2, no. 2, pp. 1-21, 1997/06/01 1997, doi: 10.1007/s00897970111a.

[5] S. Daly, K. Bhattacharya, and G. Ravichandran, "Deformation Behavior of a Shape Memory Alloy: Nitinol," in *Engineering Systems Design and Analysis*, 2008, vol. 48357, pp. 553-553.

[6] M. Es-Souni, M. Es-Souni, and H. Fischer-Brandies, "Assessing the biocompatibility of NiTi shape memory alloys used for medical applications," *Analytical and bioanalytical chemistry,* vol. 381, no. 3, pp. 557-567, 2005.

[7] W. Haider and N. Munroe, "Assessment of Corrosion Resistance and Metal Ion Leaching of Nitinol Alloys," *Journal of Materials Engineering and Performance,* vol. 20, no. 4, pp. 812-815, 2011/07/01 2011, doi: 10.1007/s11665-011-9892-5.

[8] C. Trepanier, R. Venugopalan, and A. R. Pelton, "Corrosion resistance and biocompatibility of passivated NiTi," in *Shape memory implants*: Springer, 2000, pp. 35-45.

[9] J. Mohd Jani, M. Leary, A. Subic, and M. A. Gibson, "A review of shape memory alloy research, applications and opportunities," *Materials & Design (1980-2015),* vol. 56, pp. 1078-1113, 2014, doi: 10.1016/j.matdes.2013.11.084.

[10] T. M. R. (TMR). "'Nitinol Medical Devices Market - Global Industry Analysis, Size, Share, Growth, Trends, and Forecast, 2019–2027'." Transparency Market Research (TMR). (accessed May/30, 2021).

[11] G. Savio, S. Rosso, R. Meneghello, and G. Concheri, "Geometric modeling of cellular materials for additive manufacturing in biomedical field: a review," *Applied bionics and biomechanics,* vol. 2018, 2018.
[12] M. Mahmoudi *et al.*, "On the printability and transformation behavior of nickel-titanium shape memory alloys fabricated using laser powder-bed fusion additive manufacturing," *Journal of Manufacturing Processes,* vol. 35, pp. 672-680, 2018.
[13] T. Bormann, B. Müller, M. Schinhammer, A. Kessler, P. Thalmann, and M. de Wild, "Microstructure of selective laser melted nickel–titanium," *Materials characterization,* vol. 94, pp. 189-202, 2014.
[14] H. Meier and C. Haberland, "Experimental studies on selective laser melting of metallic parts," *Materialwissenschaft und Werkstofftechnik,* vol. 39, no. 9, pp. 665-670, 2008.
[15] J.-N. Zhu, E. Borisov, X. Liang, E. Farber, M. J. M. Hermans, and V. A. Popovich, "Predictive analytical modelling and experimental validation of processing maps in additive manufacturing of nitinol alloys," *Additive Manufacturing,* vol. 38, 2021, doi: 10.1016/j.addma.2020.101802.
[16] X. Wang *et al.*, "Effect of process parameters on the phase transformation behavior and tensile properties of NiTi shape memory alloys fabricated by selective laser melting," *Additive Manufacturing,* vol. 36, 2020, doi: 10.1016/j.addma.2020.101545.
[17] J. M. Walker, C. Haberland, M. Taheri Andani, H. E. Karaca, D. Dean, and M. Elahinia, "Process development and characterization of additively manufactured nickel–titanium shape memory parts," *Journal of Intelligent Material Systems and Structures,* vol. 27, no. 19, pp. 2653-2660, 2016.
[18] C. A. Biffi, J. Fiocchi, F. Valenza, P. Bassani, and A. Tuissi, "Selective Laser Melting of NiTi Shape Memory Alloy: Processability, Microstructure, and Superelasticity," *Shape Memory and Superelasticity,* vol. 6, no. 3, pp. 342-353, 2020, doi: 10.1007/s40830-020-00298-8.
[19] H. Gu, H. Gong, D. Pal, K. Rafi, T. Starr, and B. Stucker, "Influences of Energy Density on Porosity and Microstructure of Selective Laser Melted 17-4PH Stainless Steel," 2013.
[20] M. Frotscher, P. Nörtershäuser, C. Somsen, K. Neuking, R. Böckmann, and G. Eggeler, "Microstructure and structural fatigue of ultra-fine grained NiTi-stents," *Materials Science and Engineering: A,* vol. 503, no. 1, pp. 96-98, 2009/03/15/ 2009, doi: https://doi.org/10.1016/j.msea.2008.02.059.
[21] G. Eggeler, E. Hornbogen, A. Yawny, A. Heckmann, and M. Wagner, "Structural and functional fatigue of NiTi shape memory alloys," *Materials Science and Engineering: A,* vol. 378, no. 1, pp. 24-33, 2004/07/25/ 2004, doi: https://doi.org/10.1016/j.msea.2003.10.327.
[22] M. Nematollahi *et al.*, "Laser Powder Bed Fusion of NiTiHf High-Temperature Shape Memory Alloy: Effect of Process Parameters on the Thermomechanical Behavior," *Metals,* vol. 10, no. 11, 2020, doi: 10.3390/met10111522.
[23] Y. Kim, "Fatigue Properties of the Ti-Ni Base Shape Memory Alloy Wire," *MATERIALS TRANSACTIONS,* vol. 43, no. 7, pp. 1703-1706, 2002, doi: 10.2320/matertrans.43.1703.
[24] J. Frenzel, E. P. George, A. Dlouhy, C. Somsen, M. F. X. Wagner, and G. Eggeler, "Influence of Ni on martensitic phase transformations in NiTi shape memory alloys," *Acta Materialia,* vol. 58, no. 9, pp. 3444-3458, 2010/05/01/ 2010, doi: https://doi.org/10.1016/j.actamat.2010.02.019.

[25] M. Mehrpouya, A. Gisario, A. Rahimzadeh, M. Nematollahi, K. S. Baghbaderani, and M. Elahinia, "A prediction model for finding the optimal laser parameters in additive manufacturing of NiTi shape memory alloy," *The International Journal of Advanced Manufacturing Technology,* vol. 105, no. 11, pp. 4691-4699, 2019/12/01 2019, doi: 10.1007/s00170-019-04596-z.

[26] M. Mehrpouya, A. Gisario, M. Nematollahi, A. Rahimzadeh, K. S. Baghbaderani, and M. Elahinia, "The prediction model for additively manufacturing of NiTiHf high-temperature shape memory alloy," *Materials Today Communications,* vol. 26, p. 102022, 2021/03/01/ 2021, doi: https://doi.org/10.1016/j.mtcomm.2021.102022.

[27] G. Tapia, S. Khairallah, M. Matthews, W. E. King, and A. Elwany, "Gaussian process-based surrogate modeling framework for process planning in laser powder-bed fusion additive manufacturing of 316L stainless steel," *The International Journal of Advanced Manufacturing Technology,* vol. 94, no. 9-12, pp. 3591-3603, 2017, doi: 10.1007/s00170-017-1045-z.

[28] G. Tapia, A. H. Elwany, and H. Sang, "Prediction of porosity in metal-based additive manufacturing using spatial Gaussian process models," *Additive Manufacturing,* vol. 12, pp. 282-290, 2016, doi: 10.1016/j.addma.2016.05.009.

[29] A. Solomou *et al.*, "Multi-objective Bayesian materials discovery: Application on the discovery of precipitation strengthened NiTi shape memory alloys through micromechanical modeling," *Materials & Design,* vol. 160, pp. 810-827, 2018, doi: 10.1016/j.matdes.2018.10.014.

[30] R. B. Gramacy, *Surrogates: Gaussian process modeling, design, and optimization for the applied sciences*. Chapman and Hall/CRC, 2020.

[31] A. D. Bull, "Convergence rates of efficient global optimization algorithms," *Journal of Machine Learning Research,* vol. 12, no. 10, 2011.